Deterministic aperiodic photonic crystal with a 2D array of metallic nanoparticles as polarization-sensitive dichroic filter

Igor A. Glukhov (iD), Yuliya S. Dadoenkova (iD), Florian F. L. Bentivegna (iD), and Sergey G. Moiseev (iD)

View Online   Export Citation   CrossMark

AIP
Publishing

Deterministic aperiodic photonic crystal with a 2D array of metallic nanoparticles as polarization-sensitive dichroic filter

Igor A. Glukhov,[1,2] (iD) Yuliya S. Dadoenkova,[1,2] (iD) Florian F. L. Bentivegna,[1] (iD) and Sergey G. Moiseev[2,3,a)] (iD)

AFFILIATIONS

[1]Lab-STICC (UMR 6285), CNRS, ENIB, 29238 Cedex 3 Brest, France
[2]Technological Research Institute, Ulyanovsk State University, 432017 Ulyanovsk, Russia
[3]Kotelnikov Institute of Radio Engineering and Electronics, Russian Academy of Sciences, Ulyanovsk Branch, 432011 Ulyanovsk, Russia

[a)]**Author to whom correspondence should be addressed:** moiseev@ulsu.ru

ABSTRACT

We demonstrate the possibility of using a two-dimensional array of spheroidal metallic nanoparticles embedded in a one-dimensional photonic crystal to obtain a narrow-bandpass, polarization-sensitive dichroic filter operating in the near-UV and visible domains. The optical anisotropy of the array of identically oriented nanoparticles results in two spectrally distinct plasmon resonances independently excited for two mutually orthogonal linear polarization states of light, which ensures polarization and spectral selectivity of the composite structure. The narrow transmission bands of the filter are defect modes due to a layer located at the center of the structure and hosting the nanoparticle array. In order to suppress these transmission windows, it is essential that the defect modes closely coincide with the plasmon resonances excited in the array. We show that the use of deterministic aperiodic distributed reflectors surrounding the defect layer makes it possible to adjust the spectral positions of two defect modes in two separate bandgaps in order to achieve such a coincidence. Among the various parameters governing the precise position of transmittivity windows of the filter, we establish the strong influence of the thickness of the defect layer. We also show that a strong localization of the optical field in the plane of the nanoparticle array is essential to enhance the efficiency of plasmonic excitation and obtain the desired control of the defect modes. Our study opens up possibilities for the further development of polarization-controlled nanophotonic devices.

Published under license by AIP Publishing. https://doi.org/10.1063/5.0008652

I. INTRODUCTION

Dichroic filters possess the ability to selectively transmit or reject two separate spectral bands of an incident light beam. The rejected band is usually reflected, but the concept can be extended to cases where it is absorbed. A few common applications of dichroic filters include heat control in lighting appliances, liquid-crystal-based projectors,[1] fluorescence microscopy, or photovoltaics.[2] They can also be used as high-pass filters in laser frequency multipliers, e.g., by separating the spectral components of higher harmonic generators.[3]

Dichroic filtering can be obtained in various ways, including the use of multilayered structures such as unidimensional photonic crystals (PCs). Indeed, the transmission spectrum of such structures made of periodically (but also quasi-periodically) alternating layers is known to exhibit photonic bandgaps, i.e., frequency ranges in which the propagation of electromagnetic waves is prohibited.[4,5] Moreover, breaking the periodicity of a PC by introducing one or several defect layers (made of a different material from those constituting the periodically alternating layers or simply having a different thickness) leads to the appearance of narrow peaks of high transmittivity (so-called defect modes) at frequencies located inside the photonic bandgaps. These well-established properties have been put to use in the last decades for the design of many types of PC-based reflectors and filters,[6] and the inclusion in them of, among others, reflective coatings,[7,8] all-dielectric metasurfaces[9–12] or metallic composites[13–15] have been shown to allow further control of their spectral characteristics or to introduce an additional control of those characteristics by the state of polarization of light.

It is well known that a single metallic nanoparticle (NP) can support localized surface plasmon resonances that manifest themselves through characteristic peaks in its extinction spectrum.

Similarly, the extinction spectrum of metallic NPs ordered into one-, two-, or three-dimensional arrays exhibits collective plasmon resonance response.[16–19] By carefully choosing the constitutive parameters of the NP array, one can control the optical properties of the composite structure,[13,15,20–23] and spectral and polarization-sensitive control of the resonance modes of PC-based structures hosting 3D arrays of metallic NPs can be achieved.[24–29] In those studies, polarization selectivity is realized through the use of anisotropic 3D nanocomposites—in effect, matrices hosting non-spherical metallic inclusions distributed over their entire volume. For instance, Ref. 24 reports on the design of a dichroic filter in which an anisotropic 3D metal-dielectric nanocomposite layer is sandwiched between two Bragg mirrors, and the constitutive parameters of the structure can be made to ensure the split of the incident light wave into two orthogonally polarized components at the frequencies of two defect modes. However, a significant drawback of using a 3D nanocomposite lies with the actual complexity of practically manufacturing such a material in which the shape and concentration of NPs are controlled. In addition, distributing metallic nanoparticles over the entire volume of a microresonator leads to a significant dissipation of the optical field energy, even outside the plasmon resonance spectral range, and thus to undesirable modifications of the transmission spectrum of the structure in the region of its photonic bandgaps.

For these reasons, we have chosen to use 2D arrays of nanoparticles, whose manufacturing technology is now fairly well developed,[30–34] and which lead to much less energy dissipation, as an alternative to 3D nanocomposites for functional photonic crystal structures.[35,36]

However, it is important to point out a crucial difference between the use of 2D and 3D NP distributions. In a microcavity made of a 3D nanocomposite, a localization region (antinode) of the optical field at the frequency of a defect mode will always cover a fraction of the NPs, which ensures the easy coupling of the photon and plasmon subsystems. A 2D array of nanoparticles, on the other hand, has a thickness much smaller than the optical wavelength. Consequently, its influence on the transmission spectrum of the photonic structure is determined not only by matching the frequencies of a photonic defect mode and plasmon excitation in the NPs, but also by the spatial overlap of the 2D array with a region of high optical field localization.
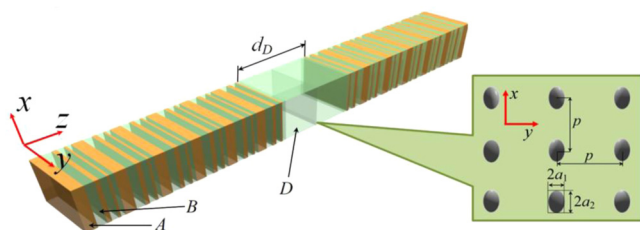

FIG. 1. Schematic of the composite photonic structure. Two symmetrical deterministic aperiodic multilayered reflectors consisting of alternate A (in orange) and B (in green) layers are separated by a layer D (thickness d_D). A 2D array of spheroidal metallic nanoparticles, characterized by the dimensions $2a_1$ and $2a_2$ of the particles and the interparticle distance p, is located at the center of the structure.

Thus, replacing a 3D composite with a 2D array of NPs is a non-trivial task that requires to carefully design the photonic crystal structure—essentially because matching plasmonic and photonic modes then becomes more complicated.

In this paper, we propose the design of a polarization-controlled dichroic filter based on the use of a single 2D array of metallic spheroidal NPs embedded in a defect layer surrounded by two reflectors. As mentioned above, using a 2D array simplifies the fabrication of such a filter and reduces energy dissipation at frequencies away from the plasmon resonances of the NPs. The working principle of such a filter is as follows. The prolate spheroidal shape of the NPs ensures that they can sustain two plasmon resonances excited at different frequencies for two mutually orthogonal polarizations of light, respectively, parallel and perpendicular to their long axis. As a result, the absorption of light at a frequency where a photonic defect mode coincides with a plasmon resonance frequency in the NP array substantially depends on its polarization. The structure of the multilayered photonic system and the anisotropic shape of the NPs are chosen so that two defect modes located in two separate bandgaps coincide with the two plasmon resonances and that the spectral interval between them is large enough to separately achieve the nearly complete suppression of either defect modes for one of the two mutually orthogonal states of polarization.

A crucial requirement of this scheme is the ability to adjust the number, location, and width of the bandgaps and defect modes of the PC in order to allow the necessary coincidence between surface plasmonic modes in the NP array and photonic defect modes in separate bandgaps. Various methods have been devised to that effect, including the design of PCs with complex defect layers,[37,38] or the external control of transmission spectra with magnetic or electric fields.[29,39,40] Another route consists in playing with the geometry of the PC. In comparison to regular, periodic, 1D PCs, multilayered structures with a complex periodicity (e.g., multi-periodic[41–44] or quasi-periodic PCs,[45–49] or even disordered multilayered structures[50]) can exhibit more bandgaps in a given frequency region of interest, as well as several defect modes in those bandgaps, which greatly expands the possibilities for their use. In this paper, we propose the use of a deterministic aperiodic PC whose complex architecture follows a set of mathematical rules[51,52] that enable the adjustment of the location of the photonic bandgaps and defect modes around the frequencies of the plasmon resonances of the NPs.

The paper is organized as follows. In Sec. II, we introduce the composite photonic structure under study and briefly present the transfer matrix method used to obtain its transmission spectrum. Section III is devoted to an extensive discussion of our calculations and highlights the conditions under which this structure can act as a polarization-dependent dichroic filter. Section IV puts forward the main conclusions of our study and some of its potential perspectives.

II. DESCRIPTION OF THE COMPOSITE PHOTONIC STRUCTURE

The structure is a resonant photonic cavity consisting of two multilayered dielectric reflectors separated by a dielectric layer D with thickness d_D and refractive index n_D, as shown in Fig. 1. A 2D

array of metallic NPs is located at the center of layer D. The reflector to the right of layer D is the mirror image of that to the left of that layer, so that the position of the NP array coincides with the center of the structure as a whole. The boundaries of all the layers are perpendicular to the z-axis of a Cartesian system of coordinates, so that $z = 0$ is the position of the first interface and the whole structure is located in the region $z \geq 0$.

Each reflector is obtained by the overlap of two distributed Bragg reflectors (DBRs) $(AB)^N$ and $(AB)^{N'}$ made of alternate nonmagnetic, isotropic, dielectric materials A and B with refractive indices n_A and n_B, respectively [Figs. 2(a) and 2(b)]. The layer thicknesses (d_A and d_B) of the first DBR and those (d'_A and d'_B) of the second DBR are chosen to satisfy the Bragg condition for two different vacuum wavelengths λ_0 and λ'_0 so that $d_{A,B} = \lambda_0/(4n_{A,B})$ and $d'_{A,B} = \lambda'_0/(4n_{A,B})$.[53] Specifically, the combination of the periodic DBRs is chosen such that the spatial variation of the refractive index in the left-hand side reflector can be written as

$$n_{left}(z) = \bar{n} + \Delta n \max[F(z), F'(z)], \quad 0 \leq z \leq L, \quad (1)$$

with

$$\bar{n} = \frac{n_A + n_B}{2}, \quad \Delta n = \frac{n_A - n_B}{2} \quad (2)$$

and

$$F(z) = \text{sgn}\left[\sin\left(\frac{2\pi}{\lambda_0}\frac{\bar{n}^2 - \Delta n^2}{\bar{n}}z\right)\cos\left(\frac{2\pi}{\lambda_0}\frac{\bar{n}^2 - \Delta n^2}{\bar{n}}z + \frac{\pi}{2}\frac{\Delta n}{\bar{n}}\right)\right]. \quad (3)$$
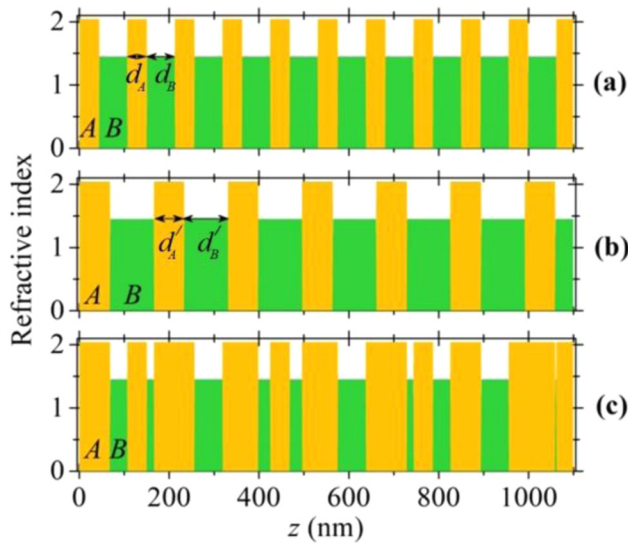

FIG. 2. Schematic of the multilayered reflector located on the left-hand side of layer D: (a) DBR $(AB)^N$ with thicknesses d_A and d_B for layers A and B; (b) DBR $(AB)^{N'}$ with thicknesses d'_A and d'_B for layers A and B; (c) deterministic aperiodic photonic crystal obtained by overlap of these DBRs as described in Eqs. (1)–(3).

The expression for $F'(z)$ can be obtained from $F(z)$ by replacing λ_0 with λ'_0.

The variation of $n_{left}(z)$ obtained on the basis of Eqs. (1)–(3) is illustrated in Fig. 2(c). The right-hand side reflector being the mirror image of the left-hand side one, the spatial dependence of its refractive index can be written as $n_{right}(z) = n_{left}(2L + d_D - z)$ for $L + d_D \leq z \leq 2L + d_D$, where L is the length of each reflector.

It is worth noticing that the combination process described by Eqs. (1)–(3) is a logical (Boolean) OR operation between the high index regions of the two periodic DBRs. It is not the only way to combine two (or more) DBRs in order to design a deterministic aperiodic reflector. Other choices could also be considered, provided, of course, the transmittivity spectra of the resulting structures exhibit photonic bandgaps and defect modes.

Calculations discussed in this section and in Sec. III are carried out for A and B layers made of ZrO_2 ($n_A = 2.02$) and SiO_2 ($n_B = 1.45$), respectively.[54] The Bragg vacuum wavelengths for DBRs $(AB)^N$ and $(AB)^{N'}$ are chosen as $\lambda_0 = 360$ nm and $\lambda'_0 = 560$ nm. Thus, the thicknesses of the layers in these DBRs are $d_A \approx 44.55$ nm, $d_B \approx 62$ nm and $d'_A \approx 69.3$ nm $d'_B \approx 96.55$ nm, respectively, so that the thickness of the unit cell is smaller in $(AB)^N$ than in $(AB)^{N'}$. The number of periods N' in DBR $(AB)^{N'}$ was chosen so that the total length $L = 2131$ nm of the reflector is the same as that of DBR $(AB)^N$ for $N = 20$.

It should be noted that for the chosen value $N = 20$, the resulting multilayered reflector does not exhibit translational symmetry, i.e., the total length of this reflector is smaller than its periodic cell (it can be shown that a periodic cell of this photonic structure is obtained for $N = 28$). However, as one can see from the results discussed below, even with $N = 20$, this deterministic aperiodic PC (and its counterpart on the right-hand side of layer D) is enough to ensure the existence of photonic bandgaps in the spectral regions encompassing the plasmon resonances in the metallic NPs. The number of layers of the dielectric mirrors surrounding the cavity was chosen on the basis of a standard criterion: it should be sufficient to allow sufficiently pronounced photonic bandgaps, i.e., bandgaps approaching ideal features (vertical boundaries and zero transmittivity). In a structure with fewer layers, the features of the photonic bandgaps are degraded—in particular, full reflectivity is not achieved. Moreover, reducing the number of layers in the reflectors leads to a decrease in the amplitude of the defect modes due to a reduction of the quality factor of the cavity.

The NPs located at the center of layer D are placed at the nodes of a 2D square lattice with period p that exhibits translational invariance along the x- and y-axes of the (xyz) Cartesian coordinate system (see Fig. 1). All NPs are prolate spheroids and similarly aligned, with their long axis parallel to the x-axis, and their shape is characterized by an aspect ratio $\xi = a_1/a_2$, where a_1 and a_2 are the half-lengths of their polar and equatorial axes, respectively ($a_1 > a_2$). The typical dimensions of the NPs and the period p of the square lattice are much smaller than the typical wavelength of the optical wave in layer D, i.e., $\{2a_1, 2a_2, p\} << \lambda/n_D$, where λ is the wavelength in vacuum.

In the following, we consider an incident plane wave in the visible regime that impinges under normal incidence on the left-hand side of the structure, at abscissa $z = 0$. The time dependence

of the electromagnetic fields is taken as $\exp(-i\omega t)$, where $\omega = 2\pi c/\lambda$ is the angular frequency of the incoming plane wave and c is the velocity of light in vacuum. The dimensions of the layers along the x- and y-axes are much larger than their thicknesses along the z-axis and are, thus, taken to be infinite in the calculations.

The optical response of such a composite multilayered photonic structure can be obtained with the transfer matrix method based on the resolution of Maxwell's equations, taking into account the constitutive equations of all materials. The overall transfer matrix of the system is obtained through the multiplication of interface matrices (derived from the boundary conditions at each interface of the system) and propagation (or dephasing) matrices in the layers.[53] The influence of the 2D NP array is described by a specific interface-like matrix whose elements are derived using a coupled-dipole approximation.[55,56] This approach allows the derivation of the reflection and refraction coefficients of the NP array surrounded on either side by an identical semi-infinite dielectric medium. Due to the prolate shape of the spheroidal NPs, these coefficients depend on the polarization state of light and on the structural parameters of the NP array itself (the shape and size of the NPs and the interparticle distance p). From the transfer matrix of the entire system, we derive transmittivities $T_{x,y} = |E_t/E_i|^2$ which, for x- or y-polarized incident light at normal incidence, relate the complex amplitudes E_i and E_t of the incident and transmitted optical electric fields. A detailed analytical derivation of the transmittivities of a similar photonic system (in particular, the treatment of the 2D NP array) can be found in Ref. 35.

III. RESULTS AND DISCUSSION

In the following, the calculated transmittivity spectra of the structure for x- and y-polarized incident light are discussed in relation to the respective spectral positions of two of its defect modes and the surface plasmon resonances in the NP array. The crucial roles played by the position of the latter within layer D and the thickness of that layer are highlighted, and the mechanism of a polarization-dependent suppression of the defect modes is detailed.

Figure 3 represents the transmittivity spectra of the structure under consideration in a near-UV and visible spectral range encompassing two neighboring photonic bandgaps (henceforth referred to as the *lower-λ* and *higher-λ* bandgaps). As in regular PCs, these bandgaps result from the geometry of the reflectors. Note that the lower-λ bandgap is narrower (with a width of approximately 56 nm) than its higher-λ counterpart (width approximately equal to 86 nm). Defect modes appear in the bandgaps due to the presence of layer D, and their number and position in the spectrum are determined by the thickness and optical characteristics and the internal structure of this composite layer.

Specifically, Fig. 3(a) shows the transmittivity spectrum of the structure without NPs in layer D, which, in this paper, we assume to be made of SiO$_2$ (as are B layers). Unless otherwise indicated (see Fig. 6 below), the thickness of that layer will be taken as $d_D \approx 485.4$ nm. This value (as well as those of the thicknesses and refractive indices of all the layers of the structure) is chosen so that two defect modes (hereinafter called L_1 and L_2, located at approximately 375 nm and 412 nm, respectively) appear in the lower-λ bandgap and one (denoted H, at 609 nm) in the higher-λ one, in
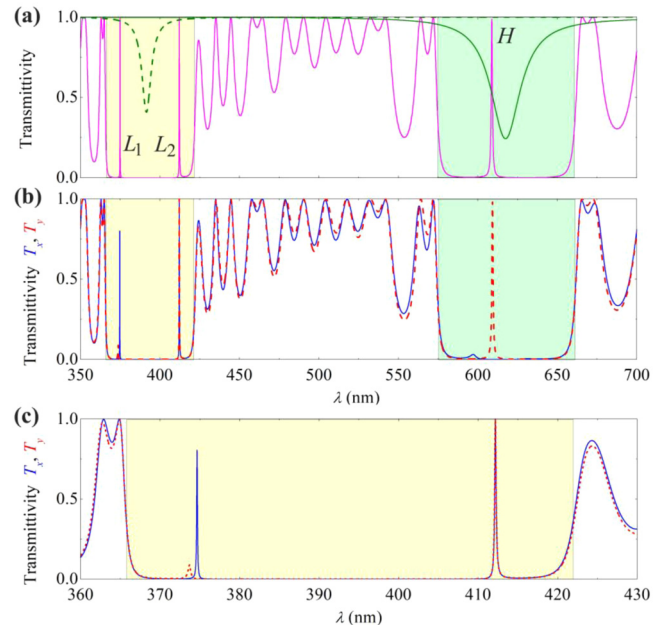

FIG. 3. Transmittivity spectra of the photonic structure: (a) without 2D array of NPs (magenta line) and for any polarization state of the incoming light wave; (b) after inclusion of a 2D array of NPs and for x-polarized (blue solid line) and y-polarized (red dashed line) incoming light wave; and (c) zoom on the lower-λ bandgap. The two defect modes in the lower-λ bandgap and the defect mode in the higher-λ bandgap are denoted as L_1, L_2, and H, respectively. The green curves superimposed to the spectrum in (a) show the transmittivity dips due to surface plasmon resonances in the sole 2D NP array embedded in a SiO$_2$ layer for x-polarized (green solid line) and y-polarized (green dashed line) incoming light, respectively.

both cases away from the bandgap edges. It should be noted that in this case, the spectrum of the photonic structure does not depend on the state of polarization of the incoming electromagnetic wave, as the structure does not include any anisotropic element.

Figure 3(a) also shows (see green lines) the transmittivity spectrum of the sole 2D NP array embedded in SiO$_2$. The array consists of silver (Ag) particles, and the interparticle distance and aspect ratio of the NPs are taken as $p = 15$ nm and $\xi = 2.5$, respectively. For $a_1 = 5$ nm, each NP is a prolate nanospheroid whose principal axes are $10 \times 4 \times 4$ nm^3 in length. The periodicity of the array and the dimensions of the NPs have been chosen so that this spectrum exhibits a broad dip inside the lower-λ (for y-polarized light) and the higher-λ (for x-polarized light) bandgaps, respectively. Those dips correspond to the polarization-sensitive excitation of a localized surface plasmon resonance in the 2D array of metallic NPs. Note that the transmission dip for x-polarized light is noticeably broader (FWHM ≈ 22 nm) than the dip observed for y-polarized light (FWHM ≈ 7 nm).

The width of the transmission dip due to the excitation of a plasmon resonance in the 2D array of nanoparticles depends on the strength of the interaction between particles and the optical wave, which, in turn, depends on a number of parameters, including the

distance between neighboring particles, their shape, and their orientation relative to the optical field. For the parameters used in this article, the strength of the interaction between the NPs and the optical wave at plasmonic resonance frequency is indeed expected to be significantly higher for x-polarized light, as that direction coincides with the axis of revolution of the NPs, for which their electric dipole moments are larger and dipole–dipole interactions are stronger.

Figure 3(b) shows the transmittivity spectra of the structure when the 2D NP array is placed at its center (as described in Sec. II and shown in Fig. 1) for the x- and y-polarization states of the incoming wave. For either of these polarization states, the plasmon resonance excited in the NPs is broad enough to encompass one of the defect modes of the structure, which leads to a significant decay and a slight blue shift of that mode, provided the polarization state of the incoming wave is well chosen. Specifically, the defect mode affected by the presence of the NPs is the one in the higher-λ bandgap for x-polarized light, whereas it is the defect mode L_1 in the lower-λ bandgap for y-polarized light [Fig. 3(c)]. We will discuss below, in relation to Figs. 4 and 5, the reason for which the defect mode L_2 remains unchanged in the presence of the NP array.

The attenuation of defect modes L_1 and H results from the absorption of light following from the excitation of a plasmon resonance in the NPs. The spectral shift they exhibit is caused by the influence of the NP array on the phase of the electromagnetic field in layer D.[36]

In Fig. 4, panel (a) represents the transmittivity spectra of x- and y-polarized light in the vicinity of defect mode H in the

higher-λ bandgap, whereas panels (b) and (c) show the spatial distribution of the square of the normalized optical field magnitude $|E(z)/E(0)|^2$ in the same spectral domain. Finally, panels (d) and (e) represent the square of the optical field magnitude normalized to its maximum value $(|E(z)/\max[E(z)]|^2)$ at the wavelength $\lambda = 609$ nm of defect mode H. For y-polarized light [panels (b) and (d)], a strong field localization is observed in layer D at this wavelength, with three almost equal optical field amplitude maxima. The thickness of that layer was chosen so that one of these maxima coincides with the position of the NP array at the center of the layer. In comparison, for x-polarized light [panels (c) and (e)], field localization appears at the lower wavelength of approximately 597 nm corresponding to the reduced and frequency-shifted defect mode (as discussed above), and the field maxima are significantly smaller than for y-polarized light [compare the transmission spectra in panel (a)].

Similar distributions of the optical field take place around the wavelength $\lambda = 375$ nm of defect mode L_1 but with a reversed polarization dependence of mode suppression as in the case of mode H. Namely, L_1 is almost completely absorbed as a result of plasmon excitation for y-polarized incident light. For x-polarized light [see inset in Fig. 3(b)], defect mode L_1 experiences a weak influence of the tail of the broad plasmon resonance centered in the higher-λ bandgap, which is why it is only slightly attenuated.

As mentioned above, the plasmon resonance of the NP array for y-polarized light [green dashed line in Fig. 3(a)] is located between the two defect modes L_1 and L_2. However, only the former is suppressed due to localized surface plasmon excitation. This can
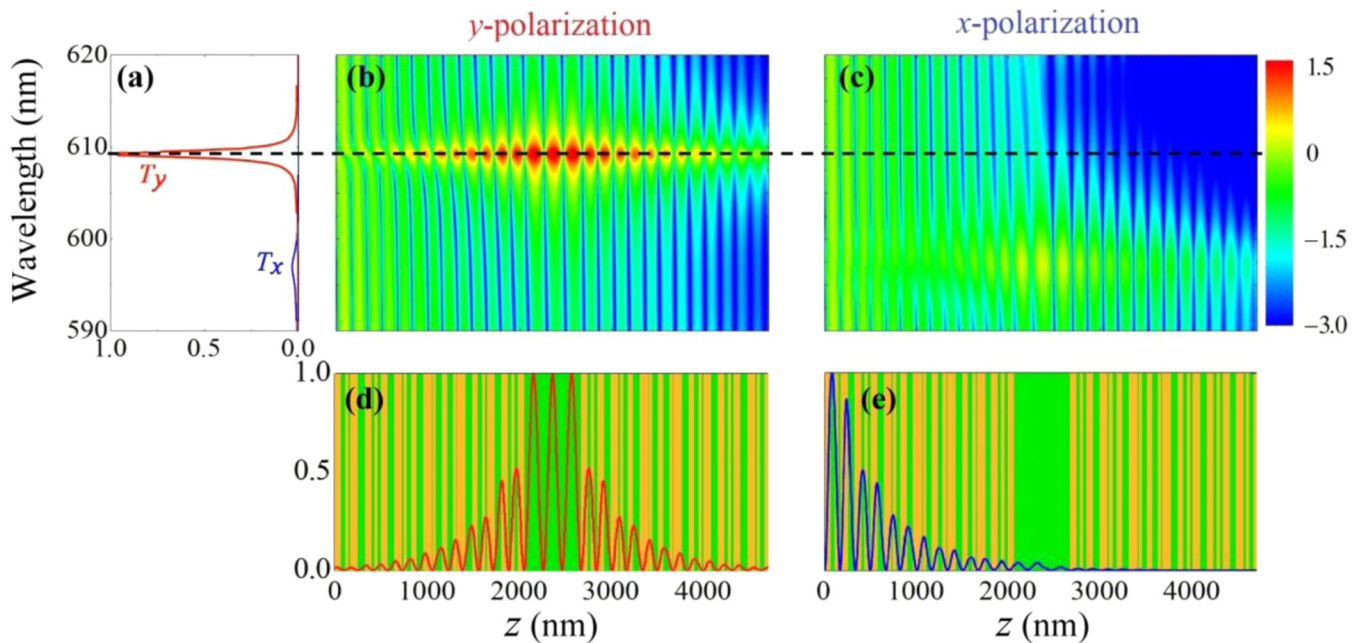

FIG. 4. Spectral characteristics of the composite PC in the vicinity of defect mode H in the higher-λ bandgap: (a) Zoom on the transmittivity spectra for x- and y-polarized light; (b) and (c) distribution of the square of the normalized optical field magnitude $|E(z)/E(0)|^2$ (in logarithmic scale) in the structure for y- and x-polarized light, respectively; (d) and (e) square of the optical field magnitude normalized to its maximum value $(|E(z)/\max[E(z)]|^2)$ at wavelength $\lambda = 609$ nm (see black dashed line in the top panels) for y- and x-polarized light, respectively. As in Figs. 1 and 2, the vertical color bars in panels (d) and (e) denote the alternate layers of the structure.
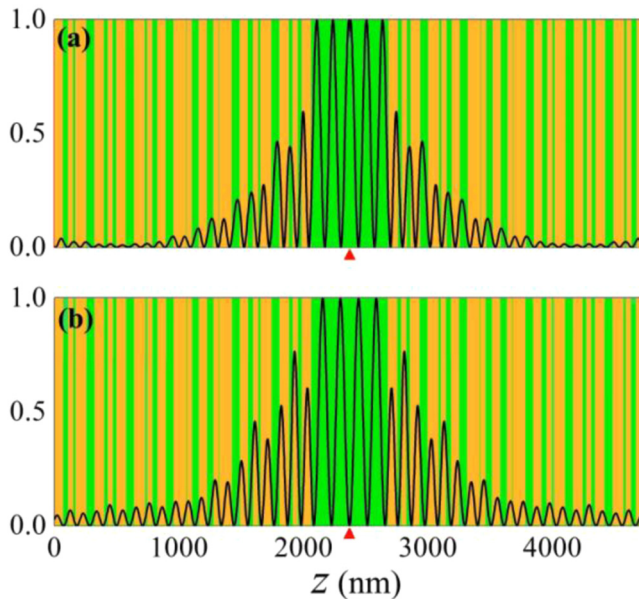
FIG. 5. Square of the optical field magnitude normalized on its maximum value ($|E(z)/\max[E(z)]|^2$) in the photonic structure without an NP array (a) at wavelength $\lambda = 375$ nm of defect mode L_1 and (b) at wavelength $\lambda = 412$ nm of defect mode L_2 for any state of polarization. The red triangles indicate the center of the photonic structure.

be explained in light of Fig. 5, where the spatial distribution of the optical field in the photonic structure without an NP array is shown at wavelength $\lambda = 375$ nm of defect mode L_1 [Fig. 5(a)] and at the wavelength $\lambda = 412$ nm of defect mode L_2 [Fig. 5(b)] for any polarization state. In the first case, the optical field exhibits a maximum at the center of the structure, which, when a 2D NP array is embedded at that position, results in a very efficient excitation of collective oscillation of the free conduction electrons in the NPs, hence a very strong suppression of defect mode L_1. In the second case, the field is almost zero at that location, and the impact of the metallic NPs on the optical field is negligible. As a consequence, defect mode L_2 is not affected by the presence of the NP array. Note that the optical field is also maximum in the plane of the NP array at wavelength $\lambda = 609$ nm of defect mode H for y-polarized light [as can be seen from Fig. 4(d)], but in that case, that mode is not suppressed by plasmon resonance, as the resonance in the NPs for y-polarized light occurs far away from 609 nm, in the lower-λ bandgap of the structure [see dashed green line in Fig. 3(a)]. Unlike what was discussed above about L_1, defect mode H does not experience much influence from the tail of the plasmon resonance centered in the lower-λ bandgap, as that resonance is significantly narrower than that centered in the higher-λ bandgap.

In effect, Figs. 3 and 4, thus, show that the polarization-dependent spectral behavior of the structure is determined both by matching the plasmon and optical defect modes and by adjusting the spatial position of the nanoparticles with respect to the antinodes of the optical field in the photonic crystal.[35]

Figure 6 illustrates the polarization-sensitive dependence of transmittivity spectra T_x and T_y in both bandgaps as functions of the thickness of layer D. As mentioned above, that thickness has until now assumed the nominal value $d_D \approx 485.4$ nm. The spectral variations of T_x and T_y are represented for thicknesses of layer D ranging from approximately 0.25 d_D to 2.25 d_D.

The behavior of the narrow transmission passbands (defect modes in the photonic bandgaps) is identical in all the cases presented in Fig. 6: as the thickness of the D layer increases, they form at the short-wavelength edge of the bandgap and shift to its long-wavelength edge, where they subsequently vanish. In each of the bandgaps, up to two defect modes can be formed simultaneously. Of particular interest is the fact that intervals of layer D thickness can be found for which defect modes are simultaneously suppressed in the lower-λ bandgap for x-polarized light and in the higher-λ bandgap for y-polarized light. This makes it possible to achieve the polarization-dependent transmittivity response required in a polarization-sensitive dichroic filter. In Fig. 6, this selective suppression of the defect modes due to the hybridization of plasmonic and photonic modes in the structure manifests itself through the absence, for a given thickness of layer D, of every second S-shaped transmission line, either for x-polarized light [Fig. 6(a)] or for y-polarized light [Fig. 6(d)], but not for both simultaneously. Note that with an increase in the strength of the interaction between the plasmonic and photonic subsystems, the photonic mode suppression occurs first and then the splitting and shift of the defect modes take place [see also Figs. 3(b) and 3(c)].

The dependence of the transmittivity spectra on the thickness of layer D deserves further discussion. For a thickness of layer D equal to d_D (vertical dashed white lines), previously discussed defect modes L_1 and L_2 in the lower-λ bandgap can be seen (dashed white circles) in Fig. 6(c), and the suppression of L_1 (but not L_2) for a y-polarized incident light beam is visible in Fig. 6(d). Similarly, the existence of defect mode H in the higher-λ bandgap (dashed white circle) and its suppression for an x-polarized light beam are clearly visible in Figs. 6(a) and 6(b), respectively. The cross sections of the transmittivity spectra along the vertical white dashed lines shown in Fig. 6 correspond to the curves presented in Figs. 3(b) and 3(c).

What Fig. 6 also shows is that a similar polarization-sensitive behavior in the lower-λ bandgap can be observed when the thickness of the layer D slightly increases from d_D up to approximately 1.25 d_D. Obviously, in so doing, the spectral positions of the defect modes change. In addition, the defect mode L_2 disappears, and the defect mode L_1 shifts toward larger wavelengths. As for defect mode H in the higher-λ bandgap, its successful suppression can be achieved for a thickness of layer D ranging from 0.9 d_D to 1.1 d_D approximately. In effect, the structure can, thus, be considered as a polarization-controlled dichroic filter when those intervals overlap, i.e., for values of the layer D thickness within [1 d_D, 1.1 d_D]. As a matter of fact, such a polarization-dependent suppression of defect modes can also occur for other thicknesses of layer D, in which case the relative spectral positions of the relevant defect modes can be different. In particular, this situation can be observed in the thickness range of [1.75 d_D, 1.85 d_D], as highlighted with solid vertical white lines and solid white circles in Fig. 6.
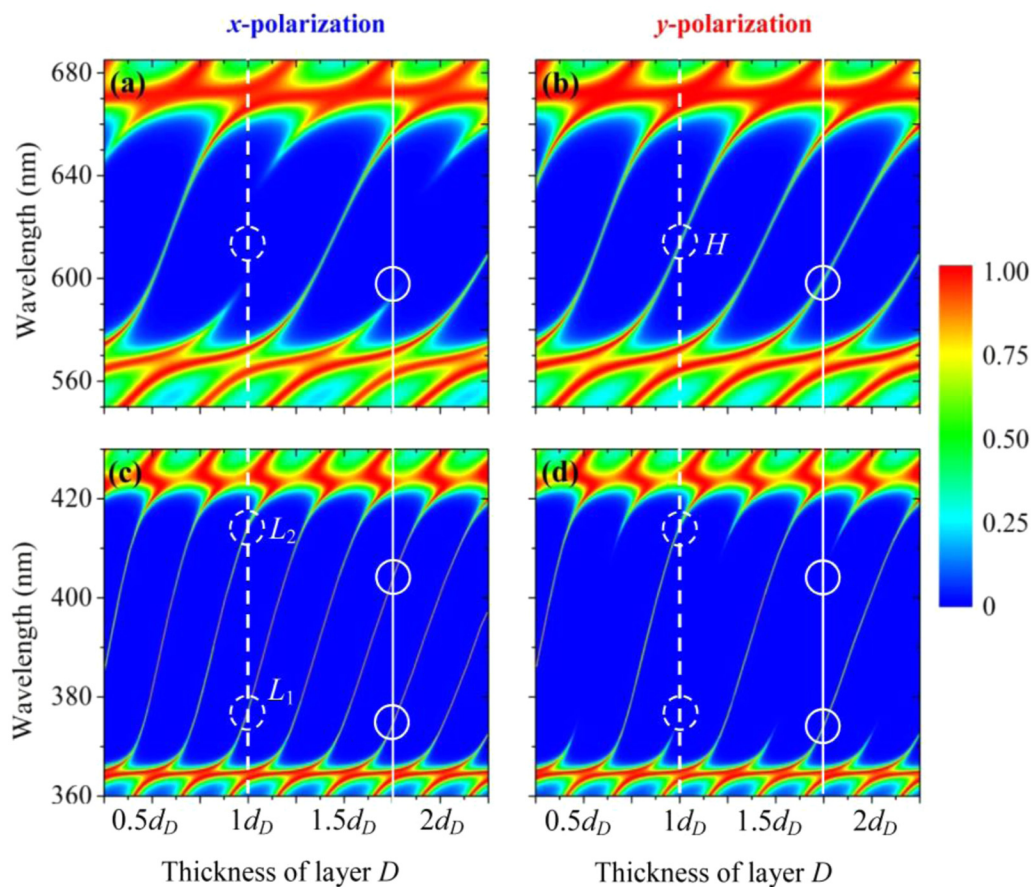
FIG. 6. Evolution of transmittivity spectra T_x [panels (a) and (c)] and T_y [panels (b) and (d)] in the higher-λ bandgap (top panels) and lower-λ bandgap (bottom panels) as functions of the thickness of layer D expressed in terms of nominal thickness d_D. The white dashed lines represent the case where that thickness is exactly equal to d_D, as in Figs. 3–5. The white solid lines represent the case where layer D thickness is equal to 1.75 d_D. The white circles denote the spectral positions of the defect modes L_1, L_2, and H discussed in the paper for these two thicknesses. The 2D array of NPs is located at the center of layer D.

Finally, it must be pointed out that the spectral characteristics of the composite photonic structure under study, based on the use of aperiodic dielectric mirrors, can vary over a rather wide range due to the large number of independent constitutive parameters that define its design (nature of the materials, layer thicknesses, rules governing the way they alternate, etc.). Thus, it is also possible to design the photonic structure so that it exhibits a single defect mode in each of the two neighboring bandgaps and to obtain a spatial distribution of the optical field such that the excitation of plasmon resonances in the 2D array of nanoparticles allows polarization-selective suppression of these defect modes. In this paper, however, we have elected to consider a structure exhibiting two defect modes in one of the photonic bandgaps. This deliberate choice has made it possible, on the one hand, to demonstrate the significance of the spatial overlap of the nanoparticle array with a region of high optical field localization in the structure and, on the other hand, to point out the possibility of selective cancellation of one of two defect modes within the same photonic bandgap.

IV. CONCLUSIONS

In this study, we have described the operating principle and governing parameters of a narrow-bandpass, polarization-sensitive dichroic filter operating in the near-UV and visible domains and consisting of a composite multilayered photonic crystal. In contrast to the photonic structure containing a 3D nanocomposite considered in a previous paper,[24] a new design for a dichroic filter combining a 2D array of metallic nanoparticles and aperiodic dielectric reflectors has been proposed. The choice of a 2D nanoparticle array, rather than a 3D nanoparticle dispersion, lends itself to a less complex fabrication process and to much less energy dissipation. The use of a deterministic aperiodic photonic crystal makes it possible to tailor the spectral position of the bandgaps and defect modes of that structure in such a way that two of these defect modes, located in separate bandgaps, can be adjusted and provide the required narrow transmittivity windows of the filter. Their non-simultaneous, polarization-sensitive suppression is achieved through

the inclusion of a composite resonant layer at the center of the photonic structure. Two surface plasmon resonances excited, for two mutually orthogonal linear states of polarization of the incoming light, in a two-dimensional array of prolate, spheroidal metallic nanoparticles embedded in that layer, can be exploited to that effect. For well-chosen values of the structural parameters of both the photonic crystal and the array of metallic nanoparticles, each of the two plasmon resonances of the latter can be made to encompass one of the two selected defect modes of the former, thus ensuring a nearly total extinction of one or the other of these modes—depending on the polarization state of the incoming light beam.

Among the various parameters governing the precise position of the transmittivity windows of the structure as a dichroic filter, we have established the strong influence of the thickness of the composite defect layer in which the array of metallic nanoparticles is embedded. Other structural parameters, however, constitute as many degrees of freedom for the design of such a filter, including the geometry of the photonic crystal, the nature of its layers, the period of the metallic nanoparticle array, the aspect ratio of the nanoparticles themselves, or the nature of the metal.

Further ways of controlling the spectral and polarization-related characteristics of that filter could be envisioned, such as the use of several metallic nanoparticle arrays or the combination of nanoparticle array(s) with other types of anisotropic media (liquid crystals with dichroic dyes, dichroic glasses, etc.). Moreover, the principles described in this study remain valid in other spectral regions, provided plasmon resonance frequencies can be made to coincide with defect modes in a multilayered photonic structure, for instance, for optical communication systems in the near-infrared domain. Other potential applications of such polarization-sensitive dichroic filters include, for instance, the development of polarization-sensitive single-photon detectors[57,58] or plasmonic absorbers and nano-sensors.[59]

ACKNOWLEDGMENTS

DATA AVAILABILITY

The data that support the findings of this study are available within the article.

REFERENCES

[1]F.-J. Ko and H.-P. David Shieh, "High-efficiency micro-optical color filter for liquid-crystal projection system applications," Appl. Opt. **39**, 1159–1163 (2000).

[2]M. Peters, J. C. Goldschmidt, P. Löper, B. Groß, J. Üpping, F. Dimroth, R. B. Wehrspohn, and B. Bläsi, "Spectrally-selective photonic structures for PV applications," Energies **3**, 171–193 (2010).

[3]J. W. Archer, "A novel quasi-optical frequency multiplier design for millimeter and submillimeter wavelengths," IEEE Trans. Microwave Theory Tech. **32**, 421 (1984).

[4]J. D. Joannopoulos, R. D. Meade, and J. N. Winn, *Photonic Crystals* (Princeton University Press, Princeton, 1995).

[5]K. Inoue and K. Ohtaka, *Photonic Crystals Physics, Fabrication and Applications* (Springer-Verlag, Berlin, 2004).

[6]Q. Gong and X. Hu, *Photonic Crystals: Principles and Applications* (Pan Stanford, 2014).

[7]D. D. Nolte, A. E. Lange, and P. L. Richards, "Far-infrared dichroic bandpass filters," Appl. Opt. **24**, 1541–1545 (1985).

[8]N. Sharma, N. Destouches, C. Florian, R. Serna, and J. Siegel, "Tailoring metal-dielectric nanocomposite materials with ultrashort laser pulses for dichroic color control," Nanoscale **11**, 18779 (2019).

[9]C.-S. Park, I. Koirala, S. Gao, V. R. Shrestha, S.-S. Lee, and D.-Y. Choi, "Structural color filters based on an all-dielectric metasurface exploiting silicon-rich silicon nitride nanodisks," Opt. Express **27**, 667–679 (2019).

[10]I. Koirala, S.-S. Lee, and D.-Y. Choi, "Highly transmissive subtractive color filters based on an all-dielectric metasurface incorporating TiO_2 nanopillars," Opt. Express **26**, 18320–18330 (2018).

[11]V. E. Babicheva, M. I. Petrov, K. V. Baryshnikova, and P. A. Belov, "Reflection compensation mediated by electric and magnetic resonances of all-dielectric metasurfaces [invited]," J. Opt. Soc. Am. B **34**, D18–D28 (2017).

[12]V. I. Zakomirnyi, A. E. Ershov, V. S. Gerasimov, S. V. Karpov, H. Ågren, and I. L. Rasskazov, "Collective lattice resonances in arrays of dielectric nanoparticles: A matter of size," Opt. Lett. **44**, 5743–5746 (2019).

[13]S. G. Moiseev, "Nanocomposite-based ultrathin polarization beamsplitter," Opt. Spectrosc. **111**, 233–240 (2011).

[14]H. Yu, Z. Liang, D. Meng, J. Tao, J. Liang, X. Su, Y. Luo, X. Xu, and Y. Zhang, "Polarization-selective dual-band infrared plasmonic absorber based on sub-wavelength gaps," Opt. Commun. **446**, 156–161 (2019).

[15]A. Muravitskaya, A. Movsesyan, S. Kostcheev, and P.-M. Adam, "Polarization switching between parallel and orthogonal collective resonances in arrays of metal nanoparticles," J. Opt. Soc. Am. B **36**, E65–E70 (2019).

[16]V. G. Kravets, A. V. Kabashin, W. L. Barnes, and A. N. Grigorenko, "Plasmonic surface lattice resonances: A review of properties and applications," Chem. Rev. **118**, 5912–5951 (2018).

[17]Y. Chu, E. Schonbrun, T. Yang, and K. B. Crozier, "Experimental observation of narrow surface plasmon resonances in gold nanoparticle arrays," Appl. Phys. Lett. **93**, 181108 (2008).

[18]M. B. Ross, C. A. Mirkin, and G. C. Schatz, "Optical properties of one-, two-, and three-dimensional arrays of plasmonic nanostructures," J. Phys. Chem. C **120**, 816–830 (2016).

[19]V. I. Zakomirnyi, I. L. Rasskazov, V. S. Gerasimov, A. E. Ershov, S. P. Polyutov, and S. V. Karpov, "Refractory titanium nitride two-dimensional structures with extremely narrow surface lattice resonances at telecommunication wavelengths," Appl. Phys. Lett. **111**, 123107 (2017).

[20]H. Hofmeister, W.-G. Drost, and A. Berger, "Oriented prolate silver particles in glass—Characteristics of novel dichroic polarizers," Nanostruct. Mater. **12**, 207–210 (1999).

[21]S. G. Moiseev, "Composite medium with silver nanoparticles as an anti-reflection optical coating," Appl. Phys. A **103**, 619–622 (2011).

[22]S. V. Eliseeva, Y. F. Nasedkina, and D. I. Sementsov, "Optical spectra of nanocomposite medium and film with metal inclusions," Opt. Spectrosc. **117**, 887–895 (2014).

[23]N. B. Leonov, S. G. Przhibel'skii, and T. A. Vartanyan, "Optical properties of plasmonic silver nanoparticles exposed to organic solvents," Opt. Quantum Electron. **49**, 127 (2017).

[24]S. G. Moiseev, V. A. Ostatochnikov, and D. I. Sementsov, "Defect mode suppression in a photonic crystal structure with a resonance nanocomposite layer," Quantum Electron. **42**, 557–560 (2012).

[25]S. Y. Vetrov, P. S. Pankin, and I. V. Timofeev, "Peculiarities of spectral properties of a one-dimensional photonic crystal with an anisotropic defect layer of the nanocomposite with resonant dispersion," Quantum Electron. **44**, 881–884 (2014).

[26]Y. Dadoenkova, I. Glukhov, S. Moiseev, V. Svetukhin, A. Zhukov, and I. Zolotovskii, "Optical generation in an amplifying photonic crystal with an embedded nanocomposite polarizer," Opt. Commun. **389**, 1–4 (2017).

[27]V. S. Gerasimov, A. E. Ershov, R. G. Bikbaev, I. L. Rasskazov, I. V. Timofeev, S. P. Polyutov, and S. V. Karpov, "Engineering mode hybridization in regular arrays of plasmonic nanoparticles embedded in 1D photonic crystal," J. Quant. Spectrosc. Radiat. Transfer **224**, 303–308 (2019).

[28]A. H. Aly, C. Malek, and H. A. Elsayed, "Transmittance properties of a quasi-periodic one-dimensional photonic crystals that incorporate nanocomposite material," Int. J. Mod. Phys. B **32**, 1850220 (2018).

[29]P. Singh, K. B. Thapa, N. Kumar, D. Singh, and D. Kumar, "Effective optical properties of the one-dimensional periodic structure of TiO_2 and SiO_2 layers with a defect layer of nanocomposite consisting of silver nanoparticle and E7 liquid crystal," Pramana-J. Phys. **93**, 50 (2019).

[30]S. Kasani, K. Curtin, and N. Wu, "A review of 2D and 3D plasmonic nano-structure array patterns: Fabrication, light management and sensing applications," Nanophotonics **8**, 2065–2089 (2019).

[31]D. B. Burckel, M. Goldflam, K. M. Musick, P. J. Resnick, G. Armelles, and M. B. Sinclair, "Coupling between plasmonic and photonic crystal modes in suspended three-dimensional meta-films," Opt. Express **28**, 10836–10846 (2020).

[32]P. M. Walmsness, T. Brakstad, B. B. Svendsen, J.-P. Banon, J. C. Walmsley, and M. Kildemo, "Optical response of rectangular array of elliptical plasmonic particles on glass revealed by mueller matrix ellipsometry and finite element modeling," J. Opt. Soc. Am. B **36**, E78–E87 (2019).

[33]A. Muravitskaya, A. Gokarna, A. Movsesyan, S. Kostcheev, A. Rumyantseva, C. Couteau, G. Lerondel, A. L. E. Baudrion, S. Gaponenko, and P.-M. Adam, "Refractive index mediated plasmon hybridization in an array of aluminium nanoparticles," Nanoscale **12**, 6394–6402 (2020).

[34]S. D. Liu, P. Yue, S. Zhang, M. Wang, H. Dai, Y. Chen, Z. Q. Nie, Y. Cui, J. B. Han, and H. J. Duan, "Metasurfaces composed of plasmonic molecules: Hybridization between parallel and orthogonal surface lattice resonances," Adv. Opt. Mater. **8**, 1901109 (2020).

[35]S. G. Moiseev, I. A. Glukhov, Y. S. Dadoenkova, and F. F. L. Bentivegna, "Polarization-selective defect mode amplification in a photonic crystal with intracavity 2D arrays of metallic nanoparticles," J. Opt. Soc. Am. B **36**, 1645–1652 (2019).

[36]S. G. Moiseev, I. A. Glukhov, V. A. Ostatochnikov, A. P. Anzulevich, and S. N. Anzulevich, "Spectra of the photonic crystal structure with a monolayer of metallic nanoparticles," J. Appl. Spectrosc. **85**, 511–516 (2018).

[37]Y. H. Lu, M. D. Huang, S. Y. Park, P. J. Kim, T.-U. Nahm, Y. P. Lee, and J. Y. Rhee, "Controllable switching behavior of defect modes in one-dimensional heterostructure photonic crystals," J. Appl. Phys. **101**, 036110 (2007).

[38]N. Ouchani, D. Bria, B. Djafari-Rouhani, and A. Nougaoui, "Defect modes in one-dimensional anisotropic photonic crystal," J. Appl. Phys. **106**, 113107 (2009).

[39]J.-X. Liu, H.-Y. Xu, Z.-K. Yang, X. Xie, Y. Zhang, and H.-W. Yang, "A research of magnetic control ferrite photonic crystal filter," Plasmonics **12**, 971–976 (2017).

[40]S. Isaacs, F. Placido, and I. Abdulhalim, "Investigation of liquid crystal Fabry–Perot tunable filters: Design, fabrication, and polarization independence," Appl. Opt. **53**, H91–H101 (2014).

[41]J. W. Klos, M. Krawczyk, Y. S. Dadoenkova, N. N. Dadoenkova, and I. L. Lyubchanskii, "Photonic-magnonic crystals: Multifunctional periodic structures for magnonic and photonic applications," J. Appl. Phys. **115**, 174311 (2014).

[42]Y. S. Dadoenkova, N. N. Dadoenkova, I. L. Lyubchanskii, J. W. Kłos, and M. Krawczyk, "Confined states in photonic-magnonic crystals with complex unit cell," J. Appl. Phys. **120**, 073903 (2016).

[43]N. N. Dadoenkova, Y. S. Dadoenkova, I. S. Panyaev, D. G. Sannikov, and I. L. Lyubchanskii, "One-dimensional dielectric bi-periodic photonic structures based on ternary photonic crystals," J. Appl. Phys. **123**, 043101 (2018).

[44]I. S. Panyaev, L. R. Yafarova, D. G. Sannikov, N. N. Dadoenkova, Y. S. Dadoenkova, and I. L. Lyubchanskii, "One-dimensional multiperiodic photonic structures: A new route in photonics (four-component media)," J. Appl. Phys. **126**, 103102 (2019).

[45]D. Qi, X. Wang, Y. Cheng, F. Chen, L. Liu, and R. Gong, "Quasi-periodic photonic crystal Fabry–Perot optical filter based on Si/SiO_2 for visible-laser spectral selectivity," J. Phys. D Appl. Phys. **51**, 225103 (2018).

[46]C. A. A. Araújo, M. S. Vasconcelos, P. W. Mauriz, and E. L. Albuquerque, "Omnidirectional band gaps in quasiperiodic photonic crystals in the THz region," Opt. Mater. **35**, 18–24 (2012).

[47]A. M. Vyunishev, P. S. Pankin, S. E. Svyakhovskiy, I. V. Timofeev, and S. Ya. Vetrov, "Quasiperiodic one-dimensional photonic crystals with adjustable multiple photonic bandgaps," Opt. Lett. **42**, 3602–3605 (2017).

[48]M. Tavakoli and Y. S. Jalili, "One-dimensional Fibonacci fractal photonic crystals and their optical characteristics," J. Theor. Appl. Phys. **8**, 113 (2014).

[49]Y. Wang, S. Jian, S. Han, S. Feng, Z. Feng, B. Cheng, and D. Zhang, "Photonic band-gap engineering of quasiperiodic photonic crystals," J. Appl. Phys. **97**, 106112 (2005).

[50]M. Bellingeri, A. Chiasera, I. Kriegel, and F. Scotognella, "Optical properties of periodic, quasi-periodic, and disordered one-dimensional photonic structures," Opt. Mat. **72**, 403–421 (2017).

[51]J. Xavier, J. Probst, and C. Becker, "Deterministic composite nanophotonic lattices in large area for broadband applications," Sci. Rep. **6**, 38744 (2016).

[52]L. Dal Negro and S. V. Boriskina, "Deterministic aperiodic nanostructures for photonics and plasmonics applications," Laser Photonics Rev. **6**, 178–218 (2012).

[53]M. Born and E. Wolf, *Principles of Optics* (Cambridge University Press, Cambridge, 1999).

[54]M. Jerman, Z. Qiao, and D. Mergel, "Refractive index of thin films of SiO_2, ZrO_2, and HfO_2 as a function of the films' mass density," Appl. Opt. **44**, 3006–3012 (2005).

[55]E. F. Kuester, M. A. Mohamed, M. Piket-May, and C. L. Holloway, "Averaged transition conditions for electromagnetic fields at a metafilm," IEEE Trans. Antennas Propag. **51**, 2641–2651 (2003).

[56]C. L. Holloway, M. A. Mohamed, E. F. Kuester, and A. Dienstfrey, "Reflection and transmission properties of a metafilm: With an application to a controllable surface composed of resonant particles," IEEE Trans. Electromagn. Compat. **47**, 853–865 (2005).

[57]D. Li and R. Jiao, "Design of a low-filling-factor and polarization-sensitive superconducting nanowire single photon detector with high detection efficiency," Photon. Res. **7**, 847–852 (2019).

[58]F. Zheng, X. Tao, M. Yang, G. Zhu, B. Jin, L. Kang, W. Xu, J. Chen, and P. Wu, "Design of efficient superconducting nanowire single photon detectors with high polarization sensitivity for polarimetric imaging," J. Opt. Soc. Am. B **33**, 2256–2264 (2016).

[59]F. Chen, L. Sun, H. Zhang, J. Li, and C. Yu, "Plasmonic absorber and nanosensor assisted by metal films coupled with hexagonal holes array," Optik **181**, 115–122 (2019).